This is an open access article published under an ACS AuthorChoice License, which permits copying and redistribution of the article or any adaptations for non-commercial purposes.

THE JOURNAL OF PHYSICAL CHEMISTRY C

Article

pubs.acs.org/JPCC

Perylene Diimide Aggregates on Sb-Doped SnO_2: Charge Transfer Dynamics Relevant to Solar Fuel Generation

Serena Berardi,*[,†] Vito Cristino,[†] Martina Canton,[†] Rita Boaretto,[†] Roberto Argazzi,[†] Elisabetta Benazzi,[†] Lucia Ganzer,[§] Rocío Borrego Varillas,[§] Giulio Cerullo,[§] Zois Syrgiannis,[⊥] Francesco Rigodanza,[⊥] Maurizio Prato,[⊥,‡,#] Carlo Alberto Bignozzi,[†] and Stefano Caramori*[,†]

[†]Dept. of Chemical and Pharmaceutical Sciences, University of Ferrara, Via Borsari 46, 44121 Ferrara, Italy

[§]IFN-CNR, Dipartimento di Fisica, Politecnico di Milano, Piazza L. da Vinci 32, 20133 Milano, Italy

[⊥]Center of Excellence for Nanostructured Materials (CENMAT), INSTM UdR di Trieste, Department of Chemical and Pharmaceutical Sciences, University of Trieste, Piazzale Europa 1, 34127 Trieste, Italy

[‡]Carbon Nanobiotechnology Laboratory, CIC biomaGUNE, Paseo de Miramón 182, San Sebastian, Spain

[#]Basque Fdn Sci, Ikerbasque, Bilbao 48013, Spain

Supporting Information

ABSTRACT: The deposition of perylene diimide-based aggregates (PDI) onto wide band gap n-type Sb-doped SnO_2 (ATO) was investigated with the aim of finding efficient and versatile dye-sensitized platforms for photoelectrochemical solar fuel generation. These ATO-PDI photoanodes displayed hydrolytic stability in a wide range of pH (from 1 to 13) and revealed superior performances (up to 1 mA/cm^2 net photocurrent at 1 V vs SCE) compared to both WO_3-PDI and undoped SnO_2-PDI when used in a photoelectrochemical setup for HBr splitting. Although ATO, SnO_2, and WO_3 are endowed with similar conduction band edge energetics, in ATO the presence of a significant density of intrabandgap states, whose occupancy varies with the applied potential, plays a substantial role in tuning the efficiency of photoinduced charge separation and collection. Furthermore, the investigation of the charge injection kinetics confirmed that, even in the absence of applied bias, ATO and WO_3 are the best substrates for the oxidative quenching of poorly reducing PDI excited states, with at least a fraction of them injecting within <200 fs. The charge-separated states recombination occurs on longer time scales, allowing for their exploitation to drive demanding chemical reactions, as confirmed in photoelectrochemical water oxidation using IrO_2-modified ATO-PDI photoanodes.

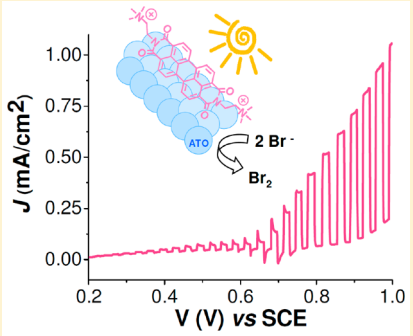

I. INTRODUCTION

In the pursuit for an efficient exploitation of renewable resources to contrast the polluting processes associated with burning coal and oil, an interesting possibility consists of the development of artificial photosynthetic devices.[1,2] As the name says, they mimic natural photosynthesis in its fundamental processes, i.e., sunlight absorption and generation of charge-separated states, which are in turn used to perform redox reactions.[3]

Water splitting[4,5] or water oxidation combined with CO_2 reduction[6,7] are among the most pursued overall reactions, given the importance of the products as alternative fuels and/or the abatement of carbon dioxide levels, by its transformation in value-added products. Common strategies involve the use of photoelectrochemical cells (PECs),[8] in which suitable photoelectrodes act as both the light harvesters and the charge separators. It is worth noting that in any proposed PEC configuration, all the involved steps must proceed in a concerted fashion in order to overcome the unproductive pathways, mainly related to the recombination of the photoproduced charges.

With regard to the water oxidation semireaction, wide band gap semiconductors (SCs), such as TiO_2[9] and WO_3,[10] have been extensively used, given the high oxidizing power of their photogenerated holes (ca. 3 V vs NHE at pH 0). However, these materials lack significant absorption of the visible part of the solar spectrum, but their performance can be improved by sensitization with suitable molecular dyes. The resulting assemblies, known as dye-sensitized photoanodes,[11] feature the separation of light absorption (due to the dye) and charge carrier transport (involving the semiconductor).[12] Photosensitizers based on metallic complexes[13] and/or organic molecules[14] with intense absorption in the visible region and suitable linking groups have been extensively used to covalently functionalize the surface of semiconducting oxides. Recently, it has been shown that even sensitizers without any specific anchoring site can adsorb/aggregate in a very stable fashion

Received: June 16, 2017
Revised: August 4, 2017
Published: August 16, 2017

ACS Publications © 2017 American Chemical Society

DOI: 10.1021/acs.jpcc.7b05928
J. Phys. Chem. C 2017, 121, 17737−17745

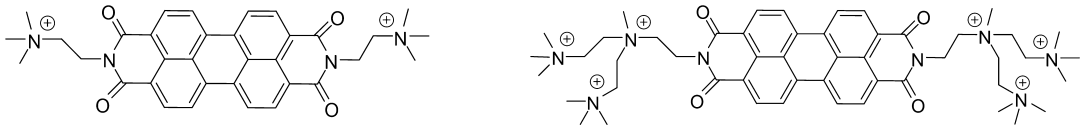

PDI PDI2

Figure 1. Structures of the photosensitizers.

onto the surfaces of these materials by hydrophobic/pi-stacking interactions.[15]

Following this latter approach, we have investigated the charge separation dynamics in different wide band gap porous semiconductors sensitized with aggregates of perylene diimide-based dyes (namely [(*N*,*N*′-bis(2-(trimethylammonium)-ethylene)-perylene-3,4,9,10-tetracarboxylic acid bis-imide)]-$(PF_6)_2$, PDI, and the hexacationic derivative PDI2, see Figure 1), with the aim of finding substrates with optimized photoinduced charge separation.

The appeal of using hydrophobic aggregates relies on the peculiar interaction with the semiconductor, which does not suffer the hydrolytic cleavage of the covalent link (see below) generally reported in the case of carboxylic or phosphonic bonds in high pH solutions.[16] Furthermore, this approach generally involves less synthetic efforts, and it does not require the use of post-treatments based on advanced techniques (e.g., atomic layer deposition[17]) or the deposition of polymeric overlayers[18] to further stabilize the linkage.

On the other hand, the charge injection by these aggregates likely proceeds through $\pi-\pi^*$ exciton migration within the molecular assembly until achieving separation at the interface between the innermost molecular surface and the semiconductor. The lack of charge transfer transitions having a precise excited state directionality will ostensibly result in a lower electronic coupling with the semiconductor surface. Thus, this mechanism of charge separation could imply a more critical competition between charge injection and other photophysical deactivation pathways, with respect to the covalent binding of traditional photosensitizers. For this reason, the pursuit of semiconductor substrates with optimized charge separation is pivotal in view of developing efficient photoanodes based on noncovalent supramolecular architectures. In particular, in this study we have revealed the superior performances of PDI-sensitized Sb-doped SnO_2 (ATO) over previously explored WO_3- and SnO_2-based photoelectrodes,[15] despite the similar conduction band energetics.

II. EXPERIMENTAL SECTION

Materials. SnO_2 colloidal solution (15% in water), 10% Sb-doped SnO_2 (50% in water), and 99.5−102.5% oxalic acid dihydrate were purchased from Alfa Aesar. Polyethylene glycol bisphenol A epichlorohydrin copolymer (15000−20000 Da), Triton-X 100, >99% $Na_2WO_4{\cdot}6H_2O$, 97% sulfuric acid, glacial acetic acid, 37% hydrochloric acid, spectroscopic grade acetonitrile (ACN), ACS grade ≥99.8% 2-propanol, $HClO_4$, $NaClO_4$, and Alconox were purchased from Sigma-Aldrich. Milli-Q water was obtained using a Millipore apparatus, equipped with 0.22 μm filters. TEC 8 (8 Ω/□) fluorine-doped tin oxide (FTO) conductive glass slides were obtained from Pilkington. Unless otherwise stated, all reagents were used as received.

Methods. AFM images were collected using a Digital Instruments Nanoscope III scanning probe microscope (Digital Instruments, CA). The instrument was equipped with a silicon tip (RTESP-300 Bruker) and operated in tapping mode. Surface topographical analysis of raw AFM images was carried out with NanoScope analysis 1.5 program.

UV−vis absorption spectra of the PDI-sensitized photoanodes were recorded with a JASCO V-570 between 800 and 350 nm (2 nm bandwidth). Unless otherwise stated, the resulting spectra were corrected for the background contribution of the respective bare SC thin films.

Electrochemical measurements were carried out in a three-electrode nitrogen-purged cell either in 0.1 M $TBAPF_6$ in ACN or in aqueous solution at pH 1 in the presence of 0.1 M Br^-. Both cyclic voltammetry (scan rates from 10 to 200 mV/s) and square wave voltammetry (10 Hz, 100 mV/s, 20−50 mV pulse width) were used to characterize the redox processes of the porous semiconductor substrates and of the PDI aggregates formed on the surface of FTO electrodes. Potentials are referred to SCE.

Photoelectrochemical measurements were carried out on a PGSTAT 30 electrochemical workstation in a three-electrode configuration, using SCE and Pt wire respectively as the reference and the counter electrode. A LOT-Oriel solar simulator, equipped with an AM 1.5 G filter, was used as the illumination source and set to 0.1 W/cm^2 incident irradiance power by means of a power meter (Newport 1918-C). *J*−*V* curves, recorded at 10 mV/s scan rate, were repeated by cycling the photoanodes until an overlapping response upon subsequent scans (stationary state) was achieved. *J*−*V* curves under shuttered illumination were acquired by manually chopping the excitation source. Unless otherwise stated, all the potential values are given versus the SCE reference electrode.

IPCE was measured in a three-electrode configuration under the monochromatic illumination generated by an air-cooled Luxtel 175 W Xe lamp, coupled to an Applied Photophysics monochromator. The resulting photocurrent, recorded at the constant potential of 0.8 V vs SCE, was measured by a PGSTAT 30 potentiostat. APCE was calculated from IPCE data corrected for the corresponding light harvesting efficiency (LHE) values.

$$\mathrm{IPCE} = 1.24 \times 10^3 \frac{J(\mu\mathrm{A/cm^2})}{\lambda(\mathrm{nm})\mathrm{P(W/m^2)}};$$

$$\mathrm{APCE} = \frac{\mathrm{IPCE}}{\mathrm{LHE}}; \quad \mathrm{LHE} = 1 - 10^{-\mathrm{A}}$$

Stationary emission spectra were measured with an Edinburgh Instruments FLS 920 spectrofluorimeter, equipped with a double emission monochromator. The photoanodes were placed in a dedicated film holder equipped with a micrometric mechanical regulation stage. In order to attain a good reproducibility, the maximum emission intensity was optimized before collecting the spectrum by tuning the angle between the electrode, the excitation beam, and the emitted

DOI: 10.1021/acs.jpcc.7b05928
J. Phys. Chem. C 2017, 121, 17737−17745

light reaching the detector. The S/N ratio was optimized by summing 10 subsequent scans with 1 nm wavelength step and a bandwidth ($\Delta\lambda$) of 4 nm. Spectra were corrected for the photomultiplier (R928P-Hamamatsu) response by using a factory built calibration file. Excitation was set to the absorption maximum of the sensitized thin films (485 nm). Background-subtracted spectra were corrected for the LHE at the excitation wavelength (λ_{exc}). Before each measurement, the sensitized photoanodes were soaked in aqueous 0.1 M $NaClO_4$ at pH 3, in order to reproduce the local ionic environment of the PEC.

Emission lifetimes of the PDI dye in ACN and adsorbed on the SC thin films were recorded with a PicoQuant Picoharp 300 time-correlated single photon counting (TCSPC) apparatus, by exciting at 460 nm with a nanoled driven by a PDL 800 B pulsing unit (40 MHz, fwhm 300 ps). Sensitized films were immersed in aqueous 0.1 M $NaClO_4$ solution at pH 3 and oriented at 45° with respect to the excitation pulse. A 470 nm cutoff filter prevented scattered excitation light from reaching the phototube. The emission was collected at 680 nm. The excited state decays were deconvolved from the excitation profile of the light source using the dedicated program Fluofit. The fluorescence decay obeyed a biexponential kinetic, whose intensity weighted average lifetime (τ_{em}) was calculated according to $\tau_{em} = \frac{A_1\tau_1^2 + A_2\tau_2^2}{A_1\tau_1 + A_2\tau_2}$, where A_1, A_2, τ_1, τ_2 are the amplitudes and lifetimes of the following function:

$$y = A_1 \exp(-t/\tau_1) + A_2 \exp(-t/\tau_2)$$

Photocurrent transients were collected by irradiating the samples with the 532 nm harmonic of a nanosecond Nd:YAG laser (Continuum Surelite II), attenuated by several neutral filters to yield an intensity of 0.6 mW/cm^2. The PDI-sensitized photoanodes were placed in a three-compartment cell and immersed in 0.1 M HBr (pH 1). An additional continuous white light bias was provided (when needed) by a LOT-Oriel solar simulator (equipped with an AM 1.5 G and a 435 nm cutoff filters) calibrated to 0.14 W/cm^2 intensity. Polarization of the photoanode was achieved using an EcoChemie PGSTAT302/N potentiostat, and the current response was sampled at 10^{-4} s intervals. The τ_{av} (amplitude-weighted) values were calculated from the biexponential fitting of the photoanodic transients, according to $\tau_{av} = \frac{A_1\tau_1 + A_2\tau_2}{A_1 + A_2}$, where A_1, A_2, τ_1, τ_2 are the amplitudes and lifetimes of the following function:

$$y = A_1 \exp(-t/\tau_1) + A_2 \exp(-t/\tau_2)$$

Femtosecond transient absorption (TA) measurements were carried out on a pump−probe setup fed by 100 fs, 2 kHz repetition rate Ti:sapphire system (Libra, Coherent) with a central wavelength of 800 nm. The pump pulses were obtained by second-harmonic generation on a 100 μm, type I β-barium borate crystal of a home-built infrared optical parametric amplifier (OPA). The so-generated pulses had a duration of ∼45 fs and a center wavelength of 485 nm. The energy was adjusted to 20 nJ, providing a fluence of 8×10^{-6} J/cm^2 on the sample. The probe pulses were obtained by white-light generation on a 3 mm thick calcium fluoride crystal, with a spectrum spanning from 350 to 700 nm. The transmitted probe beam was dispersed in a spectrometer (SP2150 Acton, Princeton Instruments) and detected using a linear image sensor driven and read out by a custom-built board from Stresing Entwicklungsbüro. The differential transmission ($\Delta T/T$) was then measured as a function of probe wavelength and pump−probe delay. For all the experiments reported in this paper, pump and probe had perpendicular polarizations; a cross-polarizer was placed in front of the detector to avoid scattered light from the pump.

Nanosecond transient absorption: Kinetic evolution of the absorption feature at 550 nm for ATO-PDI immersed in 0.1 M $NaClO_4$ (pH 3) was observed with a previously described apparatus and experimental setup,[19] by averaging the transient signal over 60 laser pulses at 532 nm. The kinetic trace, having an amplitude of ca. 1 mΔOD, was corrected for the baseline due to the monochromatic (550 nm) probe pulse averaged over 60 shots and then smoothed and fitted with a monoexponential function to calculate the charge-separated state lifetime.

Preparation of the Photoanodes. FTO cleaning was performed by sonicating the slides in Alconox solution for 10 min and in 2-propanol for a further 10 min. Colloidal WO_3 was prepared following a literature procedure[20] and then deposited via spin coating (6 s at 600 rpm, then 20 s at 2000 rpm) onto cleaned FTO slides and annealed at 550 °C for 30 min. Six successive layers were prepared, followed by 2 h soaking in 1 M H_2SO_4 and further annealing at 550 °C for 30 min. Colloidal SnO_2 was prepared following a literature procedure.[15] The resulting paste was diluted (1:2) by adding Milli-Q water and then deposited via spin coating (6 s at 600 rpm, then 20 s at 2000 rpm) onto cleaned FTO slides and annealed at 550 °C for 30 min. Colloidal Sb-doped SnO_2 (ATO) was obtained from the commercial colloidal dispersion using the same conditions described for undoped SnO_2. The resulting colloidal paste was then spin coated onto cleaned FTO slides (same conditions described for SnO_2; three subsequent depositions, each one followed by a 550 °C annealing for 30 min). Colloidal ZrO_2 was prepared and deposited onto FTO following a literature procedure.[21]

Synthesis of the Photosensitizers. The structures of perylene diimide-based dyes used in this work are reported in Figure 1. PDI was synthesized following literature procedures,[15,22,23] while a modified previously reported procedure[23,24] was used in the case of PDI2 (see Supporting Information for further details).

Dye-Sensitization of the Photoanodes. The photoanodes were soaked either in a 1 mM PDI solution in acetonitrile or in a 1 mM solution of PDI2 in DMSO, until surface saturation of the dyes was reached. The sensitized photoanodes were then rinsed with the corresponding solvent and dried under an air flow. The same conditions were adopted for surface modification of FTO for electrochemical studies.

Functionalization with IrO_2 WOC. Colloidal IrO_2 nanoparticles (NPs) solution was prepared by following literature procedures[25] and deposited onto ATO-PDI photoelectrodes by means of spin coating.[15]

III. RESULTS AND DISCUSSION

Photoelectrochemical Investigation of the Dye-Sensitized Photoanodes. In this contribution we extend our previous work on the use of PDI-sensitized photoanodes for water oxidation, in which the redox properties of the PDI's ground and excited state were assessed in ACN solution.[15] Herein we report the electrochemical and spectroscopic characterization of PDI aggregates, formed upon deposition on different substrates, showing that these species still meet the thermodynamic requirements of photoanodic assemblies. Indeed, as evidenced in Figure S1A, the PDI aggregates

DOI: 10.1021/acs.jpcc.7b05928
J. Phys. Chem. C 2017, 121, 17737−17745

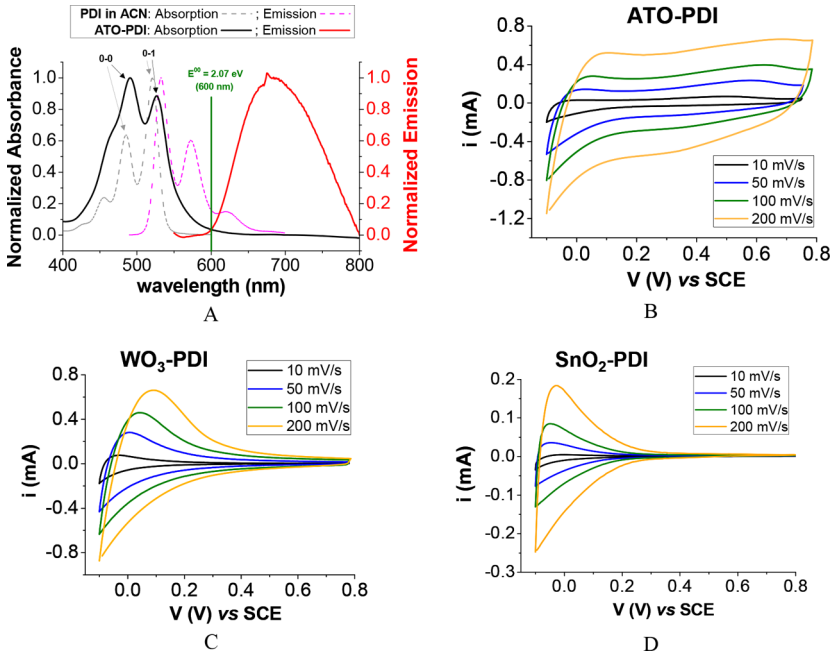

Figure 2. (A) Normalized absorption and emission spectra of PDI aggregates deposited onto ATO (solid lines) compared to those of PDI in ACN solution (dashed lines). The vibronic 0−0 and 0−1 bands in the absorption spectra are indicated with arrows. The crossing point of the ATO-PDI absorption and emission traces (E^{00}) is indicated in green. (B−D) Dark cyclic voltammetry traces of ATO-PDI (B), WO_3-PDI (C), and SnO_2-PDI (D) in 0.1 M NaBr (pH 1) using different scan rates. For ATO electrodes, the broad anodic wave observed in the 0.2−0.6 V region is assigned to intrabandgap states.

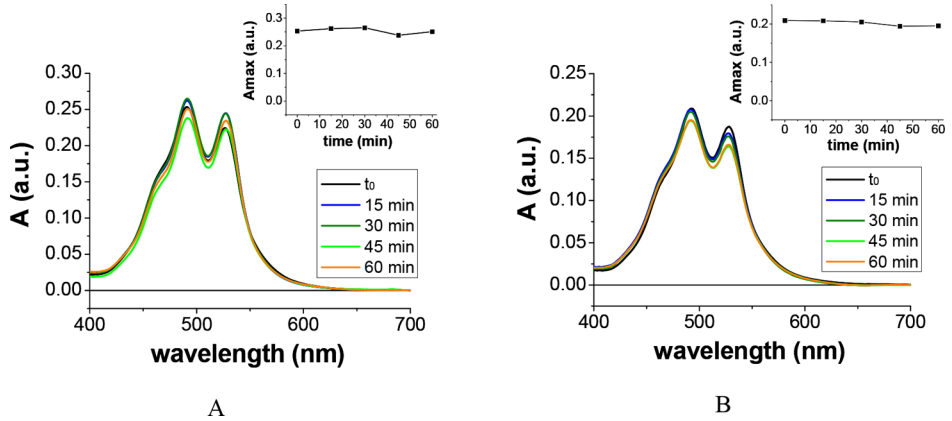

Figure 3. UV−vis spectra of ATO-PDI photoanodes after 0−60 min soaking in 0.1 M HBr, pH 1 (A) and 0.1 M NaOH, pH 13 (B). Insets: Absorbance values at λ_{max} as a function of the soaking time. All spectra corrected for the absorbance of the bare ATO.

deposited on conductive fluorine-doped tin oxide (FTO) display a E^0_{ox} potential oxidative enough (1.65 V vs SCE; unless otherwise stated, all the potential values are given versus the SCE reference electrode) to allow for the thermodynamic hole transfer to several well-known water oxidation catalysts[26,27] (needed to boost this challenging reaction), as well as for the oxidation of sacrificial agents. Conversely, the oxidation potential of PDI aggregates' excited state (E^*_{ox}) is −0.42 V, as estimated by $E^*_{ox} = E^0_{ox} - E^{00}$, E^{00} being the energy associated with the crossing point of absorption and emission spectra (see Figure 2A). It is worth noting that the calculated E^*_{ox} value matches well with the first reduction wave observed both in ACN (Figure S1B) and in aqueous solution at pH 1, where a ca. 60 mV shift to anodic potentials is observed (Figure S1C), thus ruling out a major impact of the nature of the solvent on PDI redox chemistry. The appearance of two closely spaced reductive waves, respectively assigned to formation of the mono- and direduced PDI, is qualitatively and quantitatively consistent with earlier reports dealing with the electrochemistry of perylene diimide-based dyes in solution.[28,29] We would like to emphasize that FTO electrodes display a surface chemistry rather similar to that of the investigated porous semiconductor substrates, thus providing a reliable evaluation of the aggregates' energetics relevant to charge injection.

Given the scarcely reducing power of E^*_{ox}, only semiconductors with conduction bands (CB) more positive than E^*_{ox} can be efficiently coupled with the PDI aggregates. In particular, in this work we have selected Sb-doped SnO_2 (ATO), WO_3, and SnO_2, which display a reductive current (determined by the filling of empty states close to the CB edge), with ca. 0.2 V onset potential (E_{onset}) at pH 1 (Figures 2B−D). The following continuous discharge, observed when the potential progresses toward more negative values, is due to the further CB population. An oxidation backwave, peaking

DOI: 10.1021/acs.jpcc.7b05928
J. Phys. Chem. C 2017, 121, 17737−17745

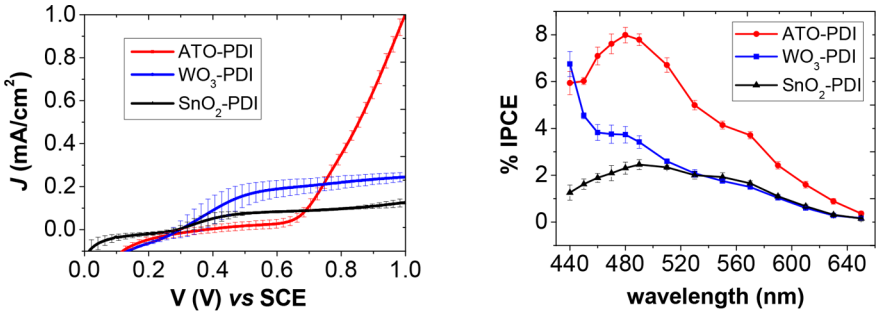

Figure 4. (A) Steady state $J-V$ curves of the PDI-sensitized photoanodes in 0.1 M HBr (pH 1); 10 mV/s scan rate; 0.1 W/cm^2 AM 1.5 G illumination (plus 435 nm cutoff filter in the case of WO_3-PDI). Average of 3 electrodes reported with the corresponding error bars. (B) IPCE curves for the PDI-sensitized photoanodes recorded at 0.8 V in 0.1 M HBr (pH 1).

between 50 mV for ATO and WO_3, and −50 mV for SnO_2, is observed when the potential scan is reversed. Notably, ATO also shows a broad and poorly resolved anodic wave between 0.2 and 0.6 V, determined by the charge extraction from a distribution of intraband-gap states (ISs) due to Sb doping. From these data, the driving force for the electron transfer from the PDI aggregates' excited state to the semiconductors' CB (ΔG_{ET}) can be estimated by $\Delta G_{ET} = -e(|E^*_{ox}| - |E_{onset}|)$, giving ca. −0.6 eV in the case of SnO_2 and WO_3. With regard to ATO, ΔG_{ET} can vary from ca. −0.6 eV (for the electron transfer to states close to the CB) to ca. −1.2 eV (for the electron transfer to the deepest emptied ISs), depending on the applied potential (vide infra).

Colloidal dispersions of the three semiconductors were deposited onto FTO electrodes, resulting in quite uniform nanostructured films consisting of particles with diameters of 100−120, 90−100, and 60−70 nm respectively for ATO, WO_3, and SnO_2, as confirmed by atomic force microscopy measurements (Figure S2). As already pointed out, the spontaneous adsorption of the perylene diimide dyes onto the surface of the semiconductors is mainly due to the precipitation of both crystalline and amorphous domains, forming H-aggregates via pi-stacking, as evidenced by the intensity reversal of the vibronic 0−0 and 0−1 bands in the absorption spectrum of ATO-PDI with respect to that of PDI in solution (Figure 2A).[30] UV−vis spectroscopy further revealed a similar dye uptake for all the substrates (Figure S3).[31]

The expected high stability of the ATO-PDI assemblies in both strong acid (0.1 M HBr) and basic (0.1 M NaOH) media over 1 h soaking has been also confirmed, as evidenced in Figure 3. The slight differences observed in the UV−vis spectra are due to the photoelectrode positioning within the sample holder.

In order to screen the charge separation and collection ability of the different dye-sensitized photoanodes, bromide (0.1 M HBr, pH 1) was selected as sacrificial agent, since it represents a redox couple with a significantly positive oxidation potential (E^0 = 0.85 V), and dark current contributions only past 0.95 V. The acidic pH was selected both to preserve WO_3 (unstable at pH > 6), and to avoid the formation of bromine oxoanions (at pH > 1), whose hydrolysis would lead to an undesired local pH rise. It is worth noting that the photoinduced HBr splitting in PEC cells represents an interesting approach,[32,33] alternative to water splitting, since its products (H_2 and Br_2) can be used in redox flow batteries to generate electricity.[34]

The photocurrents registered during the irradiation of the different PDI-sensitized photoanodes with AM 1.5 G light (0.1 W/cm^2) in the presence of Br^- are reported in Figure 4A.

At potentials >0.65 V, the ATO-PDI electrode outperforms the other two photoanodes, yielding up to 1 mA/cm^2 net photocurrent at 1 V, while WO_3-PDI and SnO_2-PDI gave plateau values of 0.25 and 0.08 mA/cm^2, respectively. However, the ATO-based photoanodes show a retarded photoanodic onset (ca. 0.65 V), ostensibly due to the recombination triggered by the intrabandgap states partially filled in the 0.2−0.6 V potential range. Further evidence of trap-mediated back recombination in this potential region is provided by the study of laser-induced photoanodic transients (see below). By comparison, the photocurrent onset is more cathodically shifted for WO_3-PDI and SnO_2-PDI (at 0.1 and 0.2 V, as better evidenced from the photocurrent transients in Figure S4).[35]

Incident photon to current efficiency (IPCE) curves of the PDI-sensitized photoanodes are reported in Figure 4B, where the action spectra are consistent with the corresponding absorption spectra of the thin films, thus confirming the involvement of the PDI molecules in the process of electron injection to the SC. The IPCEs follow, as expected, the $J-V$ curves trend, with the maximum values registered for ATO-PDI (ca. 8% at 490 nm). The low values observed for all the photoanodes are probably ascribable to incomplete quenching of the PDI excited state by electron transfer or to efficient recombination. The corresponding absorbed photon to current efficiency (APCE) spectra are, as expected, substantially independent from the absorption wavelength (see Figure S6A) achieving the best yield on ATO (12%) followed by WO_3 and SnO_2 generating ca. half that value. The above-mentioned observations are independent of the specific nature of the dye, as confirmed by the results obtained with the different, albeit structurally related, PDI2 (Figures S5 and S6B, C).

The evidence of a better charge separation on ATO is first gained by the comparative measurement of the static emission quenching of PDI aggregates loaded on the different semiconductor thin films. As shown in Figure S7, the static emission spectra of all the PDI-sensitized photoanodes consisted of a broad emission band, centered at 680 nm, significantly red-shifted with respect to the emission of PDI in ACN solution (Figure 2A), characterized by a well-defined vibronic progression. This batochromic shift, together with the lack of vibronic features, further confirms the presence of H-aggregates,[36] where the excitation may delocalize across a various number of π-interacting molecules in the form of a

DOI: 10.1021/acs.jpcc.7b05928
J. Phys. Chem. C 2017, 121, 17737−17745

traveling excitonic state, finally decaying to excimer-like states.[37] The emitting excited species (from now on generically indicated as PDI*) resulted more strongly quenched on ATO than on SnO_2 and WO_3 (which respectively display a 5.7 and 4.5 times higher fluorescence intensity, see Figure S7). This result is further corroborated by the emission lifetimes obtained by TCSPC measurements (Figure S8). Indeed, the intensity weighted lifetime (τ_{em}) of the PDI* species appears to be shorter on ATO than on WO_3 and SnO_2 (respectively 0.7 vs 1.1 and 1.2 ns, Table 1), indicative of a better electron transfer

Table 1. Intensity-Weighted Lifetimes (τ_{em}) of PDI* on the Different Metal Oxides, Measured in 0.1 M $NaClO_4$, pH 3[a]

no.	τ_{em} (intensity weighted), ns
ATO-PDI	0.699 ± 0.022
WO_3–PDI	1.179 ± 0.024
SnO_2–PDI	1.208 ± 0.058
ZrO_2–PDI	2.066 ± 0.005
PDI in ACN	4.623 ± 0.034

[a]Average values of two different electrodes, obtained by the fitting of the corresponding curves in Figure S8. τ_{em} of PDI* in ACN is also reported for sake of comparison.

into acceptor states of the former. Clearly, other deactivation pathways, not necessarily related to the electron transfer, but for example to PDI aggregates' size, exciton annihilation, and/or surface heterogeneity, might contribute to the observed quenching of the luminescence. For comparison's sake, the intensity weighted lifetimes of PDI* in ACN solution as well as onto the inert ZrO_2 substrate are also reported, in both cases evidencing the expected higher τ_{em} values, due to the lack of electron injection. It is worth noting that the observed τ_{em} trend can be used just for qualitative comparative purposes. Indeed, the instrumental time response in our TCSPC (ca. 500 ps) does not allow to extract reliable kinetic constants for the electron injection process but only to explore the relaxation of the residual population of excited states, which are long-lived due to surface heterogeneity.

To specifically address charge separation dynamics, we have measured the photoanodic transients generated by nanosecond laser excitation (7 ns full width at half-maximum, 532 nm), by recording the photocurrent response with fast (10^{-4} s sampling) chronoamperometry experiments in 0.1 M HBr, pH 1. The laser power was attenuated to generate a comparatively small perturbation with respect to the typical steady state current generated under solar simulation (to ca. 1/10 in the case of ATO), in order to extract reliable information about the dynamics in the operational cell. Photoanodic transients recorded at different applied potentials, both in the presence and in the absence of white light bias, are reported in Figure 5 for ATO-PDI and in Figure S9 for the other two substrates. In all cases, after the laser pulse, a sharp rise is observed, due to both the capacitive charging of the interface and the instantaneous (for the time scale of the experiment) electron injection and collection. In Figure S10A the dependence of these rise intensities from the applied bias is also reported.

The photocurrent decays show a biexponential time dependence, due to the progressive electron collection and recombination, which is characterized by an average lifetime (τ_{av}) extrapolated from the fittings. The applied bias dependence of τ_{av} is reported in Figure S10B, evidencing the faster

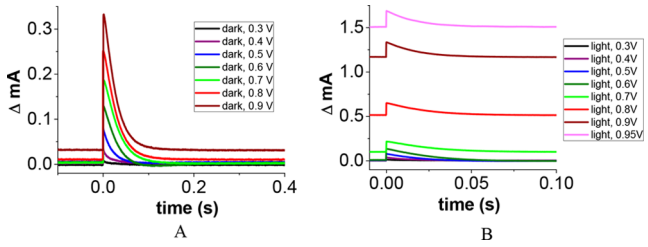

Figure 5. Photocurrent transient decays registered after the 532 nm laser excitation (0.6 mW/cm^2 intensity) under different applied bias for ATO-PDI in the absence (A) or in the presence (B) of additional white light illumination (0.14 W/cm^2 intensity). In 0.1 M HBr, pH 1.

recombination of the photogenerated $SnO_2(e^-)$-PDI(+) state with respect to the other two substrates (ca. 10–30 times lower τ_{av} for SnO_2-based photoanodes than for WO_3- and ATO-PDI). On the other hand, ATO-PDI showed the widest transients (total recovery in 0.15 s in the absence of white light bias, see Figure 5A), as well as the longest lifetimes (20–40 ms, see Figure S10B) in all the explored potential range. Furthermore, from the integration of the photocurrent transients over time, we can assess the amount of the collected photocharge, which was also plotted against the applied bias (see Figure 6A). It is

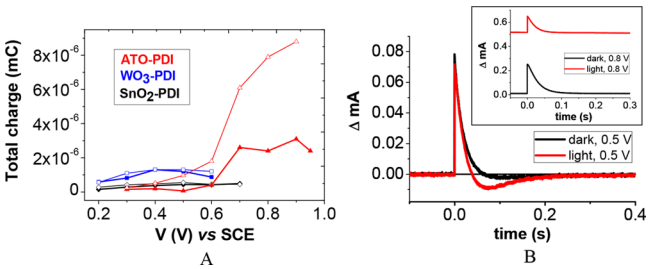

Figure 6. (A) Total collected charge as a function of the applied bias for the dye-sensitized photoanodes under pulsed 532 nm laser excitation (0.6 mW/cm^2) in the absence (empty markers) or in the presence (full markers) of white light illumination (0.14 W/cm^2). In 0.1 M HBr, pH 1. (B) Photocurrent transient decays (black traces) of ATO-PDI after 532 nm laser excitation (0.6 mW/cm^2 intensity) under 0.5 and 0.8 V (inset) applied bias. Red traces represent the laser-induced transients in the presence of continuous white light illumination of 0.14 W/cm^2 intensity. In 0.1 M HBr, pH 1.

worth noting that these transient photocharge values account for the total area delimited by the transient signals and must be summed with the proper sign (see for example Figure 6B in which part of the decay show a negative contribution, better described below).

The highest collected photocharge values are observed for ATO-PDI at >0.65 V applied bias, consistent with the steady state J–Vs, thus suggesting that the intraband states (ISs), once emptied by the applied potential, favor charge separation and collection. This assessment is further confirmed by considering ATO-PDI's decay traces at different applied potentials. Indeed, at 0.3 V (Figure S11A), regardless of the illumination conditions, the ISs are completely filled, resulting in photoanodic transients having a small amplitude with a comparatively short lifetime. At 0.5 V (Figure 6B), the ISs are only partially filled, and thus the amplitude of the transient increases, but a slow negative component appears, indicative of trap-mediated recombination. This behavior is much more evident under simultaneous white light illumination, due to the presence of a

DOI: 10.1021/acs.jpcc.7b05928
J. Phys. Chem. C 2017, 121, 17737–17745

steady state population of injected electrons and oxidized PDI at the interface. It should be noted that, in this latter case, the integrals of the positive and negative transients essentially cancel out, consistent with the lack of a steady state photoanodic response at this voltage. At 0.8 V in the dark (inset of Figure 6B), the ISs population is largely reduced, hence the negative amplitude due to back recombination component disappears. These empty states may behave as electron acceptors, whereas the applied bias accelerates charge collection over recombination. As a consequence, the anodic transient area is increased by a factor of 8 (Figure 6A), while the τ_{av} decreases (as observed in Figure S10B for $V > 0.6$ V), due to better transport. It is interesting to note that, under steady state illumination at 0.8 V (inset of Figure 6B), a partial ISs filling occurs, as the result of electron injection from PDI aggregates excited by the additional white light. This condition results in a reduced amplitude of the laser-induced transient (better evidenced by the overlapping with the dark trace in Figure S11B), as well as of the collected photocharge, suggesting that the control of the ISs occupation may allow to tune the injection quantum yield by PDI*. Conversely, the results obtained for WO_3-PDI and SnO_2-PDI point to a much less relevant effect of ISs in controlling the charge separation dynamics in these sensitized electrodes.

Ultrafast Transient Absorption Spectroscopy. In order to gain more insights on the charge injection dynamics, we have performed femtosecond transient absorption (TA) spectroscopy experiments in the absence of bias, using 485 nm pump pulses, resonant with the ground state absorption of PDI aggregates. Figure 7A shows the differential transmission ($\Delta T/T$) spectra of PDI adsorbed on the inert substrate ZrO_2. We observe a positive band at 485 nm, assigned to the photobleaching (PB) of the PDI ground state, a red-shifted positive band in the 570−610 nm range, assigned to the stimulated emission (SE) from PDI*, and a broad photoinduced absorption (PA) band, which we call PA1, at $\lambda > 620$ nm, also assigned to PDI* excited states. On the other hand, the TA spectra measured for the dye-sensitized semiconductors in the same conditions (Figures 7B−D) showed, along with the ground state bleaching (GSB) at 485 nm and the broad PA1 band at $\lambda > 620$ nm, an increased PA signal at 550 nm, which we call PA2, overlapping with and quenching the SE signal (completely in ATO and WO_3 and partially in SnO_2). We assign the enhanced PA observed at 550 nm to the SC(e^-)-PDI(+) charge-separated state generated, on the ultrafast time scale, by electron injection from the dye into the semiconductor (Figure S13). The lack of the SE in the PDI-sensitized photoanodes has been already reported for similar systems.[36]

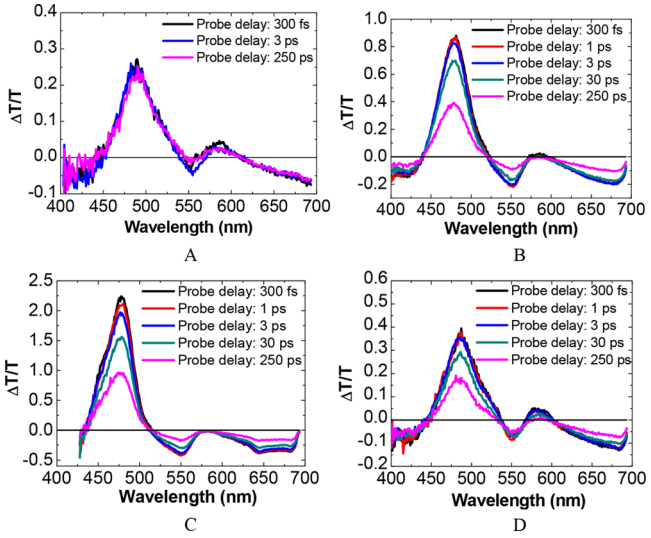

Figure 7. Transient absorption spectra of PDI-sensitized ZrO_2 (A), ATO (B), WO_3 (C), and SnO_2 (D). Femtosecond laser pulse at 485 nm.

Multiexponential fits of the TA dynamics at different probe wavelengths over the first picosecond are shown in Figure S12, and the corresponding time constants obtained by a global analysis of the data are summarized in Table S1. We observe that, while the GSB and the PA1 bands show rise times essentially limited by the ca. 45 fs instrumental resolution, PA2 shows a fast but resolved build-up. This indicates that at least a fraction[38] of the dye population is able to inject into both ATO and WO_3 on time scales of 173 ± 8 and 174 ± 5 fs, while a longer value (362 ± 12 fs) was observed for SnO_2-PDI. These evidence confirm that, even in the absence of bias, both ATO and WO_3 are the best substrates for the efficient PDI* quenching by electron transfer. ATO is, however, superior to WO_3 at potentials >0.65 V, as far as charge generation and collection is concerned.[39]

Despite the intense pump fluence typical of femtosecond experiments, charge recombination was long-lived, and the SC(e^-)-PDI(+) state recovered with a lifetime of several tens of picoseconds (174 ± 2 ps for ATO and 133 ± 1 and 165 ± 3 ps for WO_3 and SnO_2 respectively, see global analysis reported in Figure S13 and Table S1) to achieve a constant $\Delta T/T$ amplitude maintaining, in all cases, ca. 50% of the initial value. Such residual component of the charge-separated state survives far beyond the time scale of the pump probe experiment (300 ps), thus confirming the successful competition between charge separation and recombination within PDI-sensitized interfaces.

Transient measurements in the nanosecond−microsecond time scale are also consistent with the formation, upon 532 nm excitation, of the long-lived charge-separated state on ATO-PDI, absorbing at 550 nm. From the corresponding kinetic trace (Figure S14), we evidenced that the ATO(e^-)-PDI(+) state is characterized by a ca. 4 μs lifetime and undergoes to a partial recovery (ca. 50%) in the explored 20 μs time scale, thus allowing for the exploitation of the strongly oxidizing species to trigger multielectronic redox chemistry.

The proof-of-concept of the operational water oxidation by the optimized dye-sensitized photoanodes was indeed evaluated by functionalizing ATO-PDI electrodes with IrO_2 nanoparticles, acting as the water oxidation catalyst. The $J-V$ curves registered in 0.1 M $NaClO_4$ pH 3 before and after IrO_2 incorporation are reported in Figure S15, showing an augmented capacitive contribution to the total current as well as an almost doubled neat photocurrent, reaching up to 0.1 mA/cm^2 at 0.9 V in the presence of the catalyst. Even if the resulting photocurrents are still too low to be interesting in the design of an operational PEC device, we were able to prove the working principle of the proposed molecular-based photoanodes, as well as to identify the charge transfer dynamics that represent the capstone for a more complete knowledge of this kind of systems, paving the way for further improvements.

IV. CONCLUSIONS

The reported study constitutes an in-depth investigation devoted to the evaluation of platforms for the dye-sensitized

DOI: 10.1021/acs.jpcc.7b05928
J. Phys. Chem. C 2017, 121, 17737−17745

processes relevant to solar fuel generation in aqueous media. To this end, the exploitation of hydrophobic interactions to form perylene diimide-based molecular aggregates constitute an interesting solution to the hydrolytic cleavage usually observed with conventional linkers in a wide pH range. Unlike traditional photosensitizer designs, the charge injection by these aggregates proceeds through exciton migration, and their low coupling with the semiconductor surface may result in an unfavorable competition of charge injection with respect to other photophysical deactivation pathways. For this reason, finding substrates with optimized charge separation is an important task in view of developing efficient photoanodes. In particular, this study revealed the superior performances of Sb-doped SnO_2 (ATO) over previously explored WO_3- and SnO_2-based photoelectrodes having similar conduction band energetics. We also evidenced that the occupancy of intra-bandgap states on ATO play a significant role in tuning photoinduced charge separation and collection, resulting in a ca. fourfold photoanodic current for photoelectrochemical bromide oxidation with respect to WO_3. Furthermore, the investigation of the charge injection kinetics, performed in the absence of applied bias, revealed that at least a fraction of PDI* can inject on ultrafast time scales on both ATO and WO_3 (<200 fs). The following slower recombination of the charge-separated state occurs on >100 ps time scale, with a 50% fraction surviving far beyond the time scale of the experiment, up to tens of microseconds, being thus available to drive multielectronic chemical reactions.

Finally, a proof-of-concept of the possible use of the ATO-PDI as water oxidation photoanodes has been reported, provided the further functionalization with IrO_2 catalyst. Future studies will aim at the investigation of the occupancy dependence of intrabandgap states on the charge injection kinetics and the development of optimized ATO substrates to maximize light harvesting and of molecular catalysts to be coupled via specific interactions to the perylene diimide aggregates.

■ ASSOCIATED CONTENT

Supporting Information

The Supporting Information is available free of charge on the ACS Publications website at DOI: 10.1021/acs.jpcc.7b05928.

AFM images; UV−vis, IPCE, and APCE spectra; further (photo)electrochemical characterization; static and time-resolved emission spectra; transient photocurrent generation experiments; femto- and nanosecond transient absorption spectra and kinetics (PDF)

■ AUTHOR INFORMATION

Corresponding Authors

*E-mail: serena.berardi@unife.it.
*E-mail: cte@unife.it.

ORCID

Serena Berardi: 0000-0002-0275-6501
Zois Syrgiannis: 0000-0003-0345-182X

Notes

The authors declare no competing financial interest.

■ ACKNOWLEDGMENTS

The project leading to this application has received funding from the European Union's Horizon 2020 Research and Innovation Programme under the Marie Sklodowska-Curie grant agreement no. 705723. G.C. acknowledges support by the European Union Horizon 2020 Programme under grant agreement no. 696656 Graphene Flagship.

■ REFERENCES

(1) Eisenberg, R.; Nocera, D. G. Preface: Overview of the Forum on Solar and Renewable Energy. *Inorg. Chem.* **2005**, *44*, 6799−6801.
(2) Lewis, N. S.; Nocera, D. G. Powering the Planet: Chemical Challenges in Solar Energy Utilization. *Proc. Natl. Acad. Sci. U. S. A.* **2006**, *103*, 15729−15735.
(3) Barber, J. Photosynthetic Energy Conversion: Natural and Artificial. *Chem. Soc. Rev.* **2009**, *38*, 185−196.
(4) Lewis, N. S. Research Opportunities to Advance Solar Energy Utilization. *Science* **2016**, *351*, aad1920−1929.
(5) Tachibana, Y.; Vayssieres, L.; Durrant, J. R. Artificial Photosynthesis for Solar Water-Splitting. *Nat. Photonics* **2012**, *6*, 511−518.
(6) Arai, T.; Sato, S.; Kajino, T.; Morikawa, T. Solar CO_2 Reduction Using H_2O by a Semiconductor/Metal-Complex Hybrid Photocatalyst: Enhanced Efficiency and Demonstration of a Wireless System Using $SrTiO_3$ Photoanodes. *Energy Environ. Sci.* **2013**, *6*, 1274−1282.
(7) Sahara, G.; Kumagai, H.; Maeda, K.; Kaeffer, N.; Artero, V.; Higashi, M.; Abe, R.; Ishitani, O. Photoelectrochemical Reduction of CO_2 Coupled to Water Oxidation Using a Photocathode with a Ru (II)−Re (I) Complex Photocatalyst and a CoO_x/TaON Photoanode. *J. Am. Chem. Soc.* **2016**, *138*, 14152−14158.
(8) Grätzel, M. Photoelectrochemical cells. *Nature* **2001**, *414*, 338−344.
(9) Chen, X.; Mao, S. S. Titanium Dioxide Nanomaterials: Synthesis, Properties, Modifications, and Applications. *Chem. Rev.* **2007**, *107*, 2891−2959.
(10) Bignozzi, C. A.; Caramori, S.; Cristino, V.; Argazzi, R.; Meda, L.; Tacca, A. Nanostructured Photoelectrodes Based on WO_3: Applications to Photooxidation of Aqueous Electrolytes. *Chem. Soc. Rev.* **2013**, *42*, 2228−2246.
(11) Swierk, J. R.; Mallouk, T. E. Design and Development of Photoanodes for Water-Splitting Dye-Sensitized Photoelectrochemical Cells. *Chem. Soc. Rev.* **2013**, *42*, 2357−2387.
(12) Alibabaei, L.; Luo, H.; House, R. L.; Hoertz, P. G.; Lopez, R.; Meyer, T. J. Applications of Metal Oxide Materials in Dye Sensitized Photoelectrosynthesis Cells for Making Solar Fuels: Let the Molecules Do the Work. *J. Mater. Chem. A* **2013**, *1*, 4133−4145.
(13) Yu, Z.; Li, F.; Sun, L. Recent Advances in Dye-Sensitized Photoelectrochemical Cells for Solar Hydrogen Production Based on Molecular Components. *Energy Environ. Sci.* **2015**, *8*, 760−775.
(14) Mishra, A.; Fischer, M. K.; Bäuerle, P. Metal-Free Organic Dyes for Dye-Sensitized Solar Cells: From Structure: Property Relationships to Design Rules. *Angew. Chem., Int. Ed.* **2009**, *48*, 2474−2499.
(15) Ronconi, F.; Syrgiannis, Z.; Bonasera, A.; Prato, M.; Argazzi, R.; Caramori, S.; Cristino, V.; Bignozzi, C. A. Modification of Nanocrystalline WO_3 with a Dicationic Perylene Bisimide: Applications to Molecular Level Solar Water Splitting. *J. Am. Chem. Soc.* **2015**, *137*, 4630−4633.
(16) Hanson, K.; Brennaman, M. K.; Luo, H.; Glasson, C. R.; Concepcion, J. J.; Song, W.; Meyer, T. J. Photostability of Phosphonate-Derivatized, Ru^{II} Polypyridyl Complexes on Metal Oxide Surfaces. *ACS Appl. Mater. Interfaces* **2012**, *4*, 1462−1469.
(17) Vannucci, A. K.; Alibabaei, L.; Losego, M. D.; Concepcion, J. J.; Kalanyan, B.; Parsons, G. N.; Meyer, T. J. Crossing the Divide Between Homogeneous and Heterogeneous Catalysis in Water Oxidation. *Proc. Natl. Acad. Sci. U. S. A.* **2013**, *110*, 20918−20922.
(18) Wee, K.-R.; Brennaman, M. K.; Alibabaei, L.; Farnum, B. H.; Sherman, B.; Lapides, A. M.; Meyer, T. J. Stabilization of Ruthenium (II) Polypyridyl Chromophores on Nanoparticle Metal-Oxide Electrodes in Water by Hydrophobic PMMA Overlayers. *J. Am. Chem. Soc.* **2014**, *136*, 13514−13517.
(19) Ronconi, F.; Santoni, M.-P.; Nastasi, F.; Bruno, G.; Argazzi, R.; Berardi, S.; Caramori, S.; Bignozzi, C. A.; Campagna, S. Charge

DOI: 10.1021/acs.jpcc.7b05928
J. Phys. Chem. C 2017, 121, 17737−17745

Injection into Nanostructured TiO_2 Electrodes from the Photogenerated Reduced form of a New Ru(II) Polypyridine Compound: the "Anti-Biomimetic" Mechanism at Work. *Dalton Trans.* **2016**, *45*, 14109−14123.
(20) Cristino, V.; Marinello, S.; Molinari, A.; Caramori, S.; Carli, S.; Boaretto, R.; Argazzi, R.; Meda, L.; Bignozzi, C. A. Some Aspects of the Charge Transfer Dynamics in Nanostructured WO_3 Films. *J. Mater. Chem. A* **2016**, *4*, 2995−3006.
(21) Orbelli Biroli, A.; Tessore, F.; Pizzotti, M.; Biaggi, C.; Ugo, R.; Caramori, S.; Aliprandi, A.; Bignozzi, C. A.; De Angelis, F.; Giorgi, G.; Licandro, E.; Longhi, E. A Multitechnique Physicochemical Investigation of Various Factors Controlling the Photoaction Spectra and of Some Aspects of the Electron Transfer for a Series of Push−Pull Zn(II) Porphyrins Acting as Dyes in DSSCs. *J. Phys. Chem. C* **2011**, *115*, 23170−23182.
(22) Huang, Y.; Yan, Y.; Smarsly, B. M.; Wei, Z.; Faul, C. F. Helical Supramolecular Aggregates, Mesoscopic Organisation and Nanofibers of a Perylenebisimide−Chiral Surfactant Complex Via Ionic Self-Assembly. *J. Mater. Chem.* **2009**, *19*, 2356−2362.
(23) Rigodanza, F.; Tenori, E.; Bonasera, A.; Syrgiannis, Z.; Prato, M. Fast and Efficient Microwave-Assisted Synthesis of Perylenebisimides. *Eur. J. Org. Chem.* **2015**, *2015*, 5060−5063.
(24) Xu, Z.; Cheng, W.; Guo, K.; Yu, J.; Shen, J.; Tang, J.; Yang, W.; Yin, M. Molecular Size, Shape, and Electric Charges: Essential for Perylene Bisimide-Based DNA Intercalator to Localize in Cell Nuclei and Inhibit Cancer Cell Growth. *ACS Appl. Mater. Interfaces* **2015**, *7*, 9784−9791.
(25) Hara, M.; Waraksa, C. C.; Lean, J. T.; Lewis, B. A.; Mallouk, T. E. Photocatalytic Water Oxidation in a Buffered Tris (2, 2′-bipyridyl) Ruthenium Complex-Colloidal IrO_2 System. *J. Phys. Chem. A* **2000**, *104*, 5275−5280.
(26) McCrory, C. C.; Jung, S.; Peters, J. C.; Jaramillo, T. F. Benchmarking Heterogeneous Electrocatalysts for the Oxygen Evolution Reaction. *J. Am. Chem. Soc.* **2013**, *135*, 16977−16987.
(27) Llobet, A. *Molecular Water Oxidation Catalysis*; John Wiley & Sons: New York, 2014.
(28) Lee, S. K.; Zu, Y.; Herrmann, A.; Geerts, Y.; Müllen, K.; Bard, A. J. Electrochemistry, Spectroscopy and Electrogenerated Chemiluminescence of Perylene, Terrylene, and Quaterrylene Diimides in Aprotic Solution. *J. Am. Chem. Soc.* **1999**, *121*, 3513−3520.
(29) Chen, Z.; Debije, M. G.; Debaerdemaeker, T.; Osswald, P.; Würthner, F. Tetrachloro-substituted Perylene Bisimide Dyes as Promising n-Type Organic Semiconductors: Studies on Structural, Electrochemical and Charge Transport Properties. *ChemPhysChem* **2004**, *5*, 137−140.
(30) Han, J. J.; Shaller, A. D.; Wang, W.; Li, A. D. Architecturally Diverse Nanostructured Foldamers Reveal Insightful Photoinduced Single-Molecule Dynamics. *J. Am. Chem. Soc.* **2008**, *130*, 6974−6982.
(31) It is worth noting that in the case of the dye-sensitized WO_3 photoelectrodes, the absorption spectra are the sum of the contributions of both the molecular dye and the bare WO_3 (for $\lambda <$ 460 nm).
(32) Levy-Clement, C.; Heller, A.; Bonner, W.; Parkinson, B. Spontaneous Photoelectrolysis of HBr and HI. *J. Electrochem. Soc.* **1982**, *129*, 1701−1705.
(33) Khaselev, O.; Turner, J. A. Photoelectrolysis of HBr and HI Using a Monolithic Combined Photoelectrochemical/Photovoltaic Device. *Electrochem. Solid-State Lett.* **1999**, *2*, 310−312.
(34) Cho, K. T.; Tucker, M. C.; Ding, M.; Ridgway, P.; Battaglia, V. S.; Srinivasan, V.; Weber, A. Z. Cyclic Performance Analysis of Hydrogen/Bromine Flow Batteries for Grid-Scale Energy Storage. *ChemPlusChem* **2015**, *80*, 402−411.
(35) It is worth noting that for the WO_3-PDI photoanodes an additional 435 nm cutoff filter is needed in order to limit the contribution of the bare material to the total photocurrent, as well as to preserve the dye from the oxidation by the WO_3 valence band holes. For sake of comparison, ATO-PDI and SnO_2-PDI photoanodes were also tested in these conditions (even if the direct band gap excitation using the AM 1.5 G light is negligible for these substrates), evidencing a <20% decrease of the photocurrents (Figures S4B and D).
(36) Lindquist, R. J.; Phelan, B. T.; Reynal, A.; Margulies, E. A.; Shoer, L. E.; Durrant, J. R.; Wasielewski, M. R. Strongly Oxidizing Perylene-3, 4-Dicarboximides for Use in Water Oxidation Photoelectrochemical Cells. *J. Mater. Chem. A* **2016**, *4*, 2880−2893.
(37) Yoo, H.; Yang, J.; Yousef, A.; Wasielewski, M. R.; Kim, D. Excimer Formation Dynamics of Intramolecular π-Stacked Perylenediimides Probed by Single-Molecule Fluorescence Spectroscopy. *J. Am. Chem. Soc.* **2010**, *132*, 3939−3944.
(38) Griffith, M. J.; Sunahara, K.; Wagner, P.; Wagner, K.; Wallace, G. G.; Officer, D. L.; Furube, A.; Katoh, R.; Mori, S.; Mozer, A. J. Porphyrins for Dye-Sensitised Solar Cells: New Insights into Efficiency-Determining Electron Transfer Steps. *Chem. Commun.* **2012**, *48*, 4145−4162.
(39) At the present time, femtosecond-TAS measurements under electrochemical polarization cannot be performed with our setup. The direct observation of the effect of ISs occupation on charge injection will be addressed in a future contribution.

DOI: 10.1021/acs.jpcc.7b05928
J. Phys. Chem. C 2017, 121, 17737−17745